PHYSICAL REVIEW B **90**, 081402(R) (2014)

Origin of the insulating state in exfoliated high-T_c two-dimensional atomic crystals

L. J. Sandilands, A. A. Reijnders, A. H. Su, and V. Baydina
Department of Physics, 60 St. George Street, Toronto, Ontario, Canada M5S 1A7

Z. Xu, A. Yang, and G. Gu
Condensed Matter Physics and Materials Science Department, Brookhaven National Laboratory, Upton, New York 11973-5000, USA

T. Pedersen and F. Borondics
Canadian Light Source, Saskatoon, Saskatchewan, Canada S7N 2V3

K. S. Burch
Department of Physics, Boston College, Chestnut Hill, Massachusetts 02467, USA

(Received 24 October 2012; revised manuscript received 22 May 2014; published 7 August 2014)

We present the results of an optical spectroscopic study of two-dimensional atomic crystals of the high-temperature superconductor $Bi_2Sr_2CaCu_2O_{8+\delta}$. Our measurements reveal a pronounced suppression of the optical conductivity $\sigma_1(\omega)$ with thickness. Using an effective medium approximation, we interpret this in terms of an insulating surface layer. The surface layer explains the insulating behavior previously observed in exfoliated $Bi_2Sr_2CaCu_2O_{8+\delta}$ and has implications for future studies and potential applications of these materials.

DOI: 10.1103/PhysRevB.90.081402 PACS number(s): 74.72.Gh, 73.22.−f, 74.25.Gz, 78.30.Er

I. INTRODUCTION

Mechanical exfoliation of layered crystals has recently emerged as a new approach to producing unusual electronic materials, with the most prominent examples being graphene [1] and single-layer MoS_2 [2,3]. In pioneering work, Novoselov and collaborators showed that this method can be used to synthesize a wide array of ultrathin films (termed "two-dimensional atomic crystals"), including single unit cell crystals of the high-T_c cuprate superconductor $Bi_2Sr_2CaCu_2O_{8+\delta}$ (BSCCO) [4]. Besides enabling a variety of experiments [5], such as electrostatic gating [3,6], these materials can have electronic properties that differ markedly from the bulk [7,8]. Intriguingly, single-layer BSCCO was found to be insulating, in contrast to the metallic behavior observed in ultrathin molecular beam epitaxy (MBE)-grown LSCO films [9,10], as well as the expectation that the physics of the cuprates is intrinsically two dimensional (i.e., a property of a single copper oxygen plane). To better understand this apparent contradiction, we have investigated the optical properties of two-dimensional BSCCO atomic crystals.

The electronic properties of the cuprates [11–13] and exfoliated materials [7,14] in general are often probed through optical methods. Indeed, optical spectroscopy is an ideal tool for studying exfoliated BSCCO, as it provides access to the carrier dynamics and electronic structure [15]. This technique also has the advantage of not requiring nanofabrication (i.e., photoresists, solvents, and other chemicals) and is insensitive to contact resistance or extended defects that might be expected to influence DC measurements. In this Rapid Communication, we present the results of an optical study of exfoliated BSCCO of various thicknesses. Our measurements indicate pronounced changes in the optical properties with thickness. An effective medium approximation (EMA) that includes an insulating surface layer gives a good account of our thickness dependent data. The presence of an insulating surface explains the previous observation of insulating behavior in single-layer exfoliated BSCCO and emphasizes the fragility of these samples [4].

The paper is organized as follows: Section II details the exfoliated BSCCO samples and experimental methods used in our optical study. In Sec. III, we discuss how the optical constants of exfoliated BSCCO evolve as a function of thickness. Section IV describes how the data can be understood using a simple effective medium approximation (EMA), which assumes that a region near the surface of the sample has become insulating. Finally, we present our conclusions in Sec. V.

II. SAMPLE AND EXPERIMENTAL DETAILS

Two-dimensional atomic crystals of BSCCO were deposited, via the mechanical exfoliation technique [4,16,17], on 350 μm thick silicon substrates capped with 280 nm of silicon dioxide (Silicon Quest International). The optimally doped bulk crystals used in the deposition were grown by the traveling floating zone method and have typical transition temperatures of 90 K [18]. Prior to exfoliation, the substrates were prebaked at 425 K for 15 min in an effort to minimize the amount of adsorbed water at the BSCCO/SiO_2 interface, and the entire procedure (substrate baking and exfoliation) was performed in a dry atmosphere. Large (greater than 20 × 20 μm in area) samples were then identified through optical microscopy [16] and stored in a vacuum prior to measurement at the Canadian Light Source. The film thickness was established with a Digital Instruments Nanoscope III atomic force microscope (AFM) operating in contact mode. Sample thicknesses typically range from 10 to 200 nm.

It is worth noting at this point that our exfoliated BSCCO samples have been characterized by various experimental techniques and confirmed to be well-defined single crystals that retain the symmetries of the bulk, with no evidence for structural granularity or any drastic changes in the lattice. First, transmission electron microscopy (TEM) studies have

demonstrated that BSCCO two-dimensional (2D) atomic crystals are monocrystalline and have the same crystal structure as bulk [4]. This was further confirmed by Raman scattering and x-ray Laue microscopy experiments [16,19,20]. Raman scattering selection rules (i.e., whether or not an excitation can be observed) follow from the translational and point group symmetries of the lattice. Translational symmetry means that only $q = 0$ processes can be observed, while point group symmetry impose certain polarization dependences. In a previous unpolarized Raman study [19], Wang *et al*. studied scattering due to phonons as a function of thickness. They found that the number and frequency of these modes was unchanged with thickness, meaning that the lattice translational symmetry and dynamics are unperturbed in exfoliated BSCCO. We have also studied the two-magnon feature in underdoped exfoliated BSCCO using polarized Raman microscopy [16]. While this feature was blueshifted and enhanced compared to bulk, its polarization dependence was unaltered with thickness, meaning the pseudotetragonal symmetry of the BSCCO lattice is also unchanged. Finally, x-ray Laue microdiffraction measurements show a diffraction pattern unchanged from bulk, save for subtle changes associated with the incommensurate superstructure, demonstrating unequivocally that our BSCCO films are single crystal with the c axis oriented normal to the substrate surface [20].

Optical measurements of the BSCCO/SiO_2/Si/SiO_2 samples [shown schematically in the inset of Fig. 3(c)] were performed at the Canadian Light Source Mid-IR beamline at room temperature with 16 cm^{-1} resolution using a Bruker Hyperion infrared microscope equipped with a 15× [0.4 numerical aperture (NA)] objective, a Bruker Vertex 80v spectrometer, and a liquid-nitrogen-cooled HgCdTe detector. The spectra are referenced to a nearby bare region of the substrate in order to minimize errors due to system drift or alignment. A schematic of the measurement geometry is shown in the inset of Fig. 3(c). Given the orientation of our films as determined from Raman microscopy, this experimental geometry is sensitive to the *ab*-plane optical constants. These measurements are reproducible to within 1.5% and 0.5% for transmittance and reflectance, respectively. This reproducibility in turn determines the error bars in the spectral weight shown in Fig. 3(c).

The reflectance and transmittance data are shown in Fig. 1, where the transmittance ratio is seen to increase with reduced sample thickness, while the reflectance decreases. This trend is consistent with the expectation that reducing the thickness of an absorbing sample should lead to an increased transmittance. Indeed, the majority of this effect in our data is due to the change in sample thickness. In order to examine any thickness dependence of the BSCCO itself, extracting the optical conductivity $\hat{\sigma}(\omega)$ is required.

Accurate knowledge of the substrate optical constants is needed to analyze the measurements of the multilayer structures described above. Similarly, the optical properties of our bulk BSCCO crystals need to be well established if any changes with thickness are to be identified. We therefore measured the optical response of the "parent" BSCCO crystals and of the oxidized silicon substrates. The optical properties of the substrate were determined using a combination of reflectance, transmittance, and ellipsometric measurements,

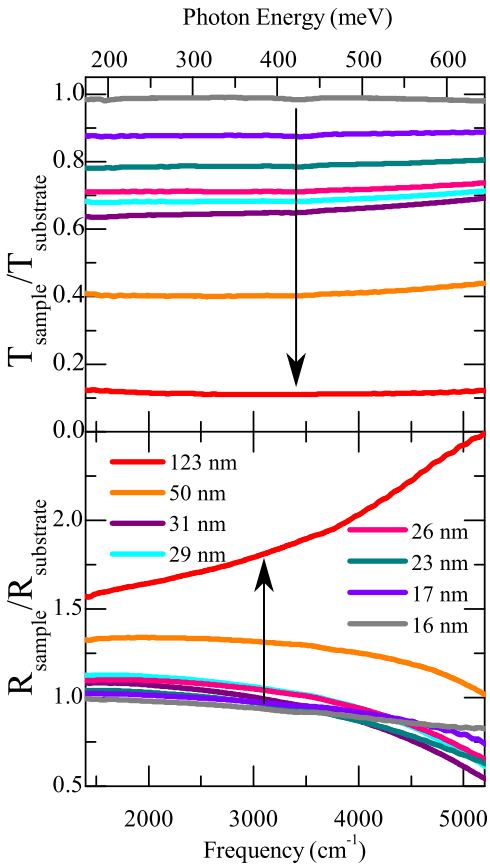

FIG. 1. (Color online) Top: Transmittance $T_{sample}/T_{substrate}$ of exfoliated BSCCO. Bottom: Reflectance $R_{sample}/R_{substrate}$ of the same samples. The sample thicknesses are listed in the legend of the bottom panel. The arrows indicate the trends in the data with decreasing thickness.

while the response of bulk BSCCO was extracted from broadband reflectivity data. The reflectance and transmittance data were collected in the range of 80–11 000 cm^{-1} at room temperature using a Bruker Vertex 80v spectrometer equipped with a custom sample space that supports simultaneous measurement of reflectance and transmittance [21]. For reflectance referencing, we used a gold mirror, and for the BSCCO a standard *in situ* gold overcoating technique was employed [22]. Ellipsometric measurements of the substrates were performed using a Woolam VASE spectroscopic ellipsometer in the range 6000–36 000 cm^{-1}. The optical constants of BSCCO were determined by extending the measured reflectance to higher frequencies using previously published data [13] and applying a Kramers-Kronig analysis. For the oxidized silicon substrates, the reflectance, transmittance, and ellipsometric data were modeled using the Woolam VASE software. The optical constants of the Si and SiO_2 layers were parametrized using an oscillator model which was then adjusted to match the experimental data. The results obtained in this way are consistent with reported measurements of BSCCO, silicon, and silicon dioxide [13,23,24]. To determine the optical constants of the exfoliated BSCCO from our microscopy data, we used a multilayer model implemented with the REFFIT software package [25]. The model allows for multiple reflections in the BSCCO and SiO_2 layers but not in the silicon substrate, as

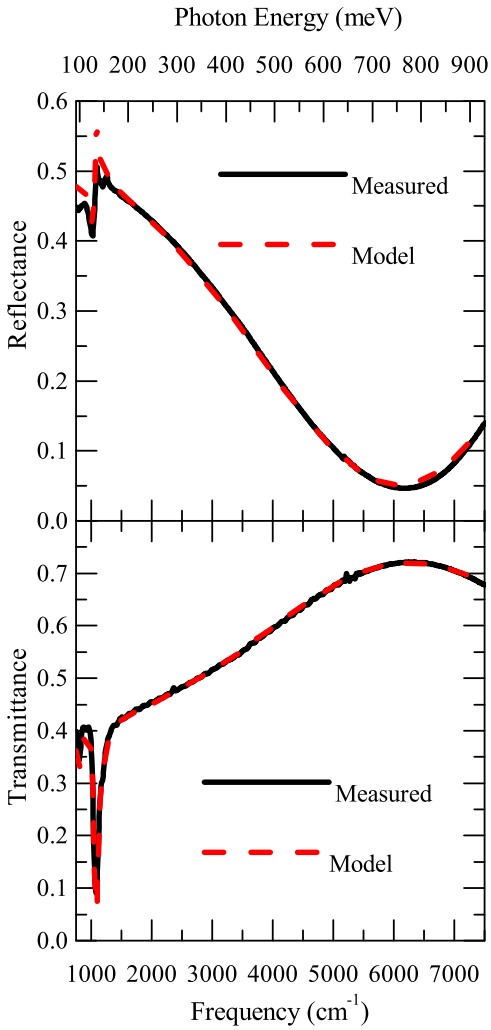

FIG. 2. (Color online) Top: Reflectivity data and model fit for a 23 nm exfoliated sample. The data is in black and the fit in red. Bottom: Measured and model transmittance for the same sample. At low frequencies near 1250 cm^{-1}, sharp features due to a SiO_2 phonon are visible in both reflectance and transmittance. The broad reflectance minimum and transmittance maximum near 6000 cm^{-1} are due to interference effects in the SiO_2 layer.

Fabry-Pérot effects from the substrate are not visible at our experimental resolution of 16 cm^{-1}. The thicknesses of the BSCCO layers were fixed to the values measured with AFM while the SiO_2 thickness was set to 280 nm, according to the manufacturer's specifications and confirmed by our ellipsometry measurements. To model the complex optical constants of the BSCCO samples, we used a Kramers-Kronig consistent variational dielectric function [26], which was then adjusted to reproduce the experimental data. Example reflectance and transmittance data for a 23 nm film are shown in Fig. 2. The minimum (maximum) in the reflectance (transmittance) is due to Fabry-Pérot effects in the oxide layer, while the sharp feature near 1250 cm^{-1} is a SiO_2 phonon. The extracted BSCCO optical constants above 5200 cm^{-1} are sensitive to the thickness and optical constants of the oxide layer used in the multilayer model. In addition, SiO_2 has several strong infrared-active phonons below 1400 cm^{-1}. These features can lead to artifacts in the BSCCO optical constants and so we limit our discussion to the frequency range 1400–5200 cm^{-1}.

III. OPTICAL RESPONSE OF EXFOLIATED BSCCO

The end results of the measurement and analysis procedure described above are the optical constants of exfoliated BSCCO. In considering the optical response of our samples, we focus on the real parts of the complex conductivity ($\hat{\sigma} = \sigma_1 + i\sigma_2$) and the complex dielectric function ($\hat{\epsilon} = \epsilon_1 + i\epsilon_2$). The real parts of these quantities are finite frequency generalizations of the DC conductivity and static dielectric constant, respectively, and reflect the carrier dynamics and

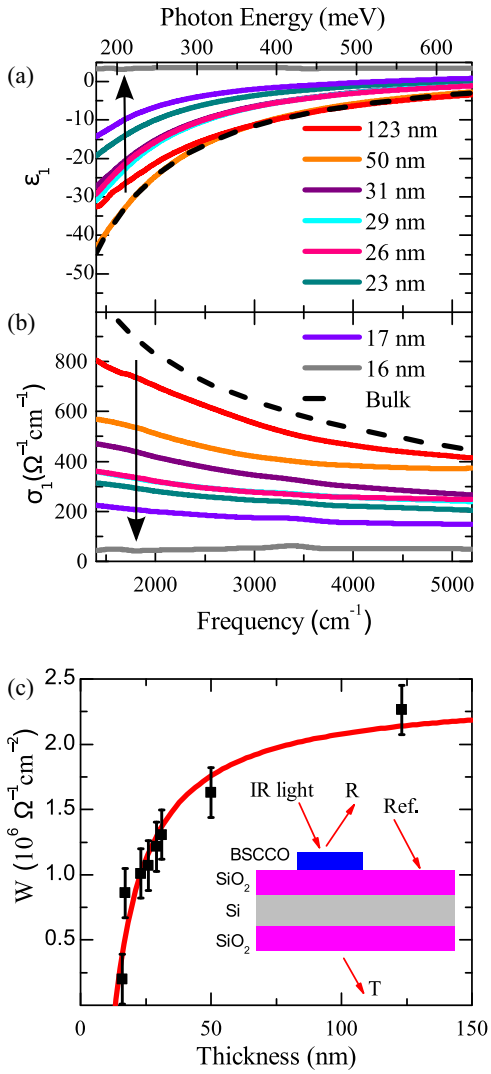

FIG. 3. (Color online) Optical properties of exfoliated BSCCO films. (a) The real part of the dielectric function ϵ_1. (b) The real part of the optical conductivity σ_1. The arrow indicates the trend of decreasing conductivity with decreased film thickness. (c) The spectral weight W integrated from 1400 to 5200 cm^{-1}. In (c), the data is shown in black while the EMA expression for W is shown in red. The color coding is consistent between (a) and (b). A schematic of the measurement geometry is shown in the inset of (c). The overall decrease in σ_1 and increase in ϵ_1 signals that the BSCCO 2D atomic crystals are becoming less metallic with decreasing thickness.

electronic structure of the exfoliated BSCCO. The dielectric function (ϵ_1) and optical conductivity (σ_1) of the exfoliated cuprate samples and of a bulk crystal are displayed in Figs. 3(a) and 3(b), respectively.

The optical functions σ_1 and ϵ_1 of the 123 nm sample display Drude-like behavior that is the spectroscopic signature of metallic transport. This Drude mode manifests itself in the real part of the optical conductivity σ_1 as a zero frequency peak with a width given by the free carrier scattering rate ($1/\tau$) and a spectral weight proportional to the squared plasma frequency $\omega_p^2 \propto (n/m_b)$, where n is the carrier density and m_b the optical mass [27]. This mode also leads to a negative ϵ_1 that reaches its most negative value at $\omega = 0$. Similar to σ_1, the finite frequency magnitude of the Drude mode in ϵ_1 is strongly affected by the plasma frequency. As seen in Figs. 3(a) and 3(b), thinner exfoliated samples reveal a σ_1 that is systematically reduced and an ϵ_1 that is increased. These results indicate a suppression of metallicity. The thinnest samples measured, 16 and 12 nm (not shown), reveal a flat, featureless σ_1 and a positive ϵ_1, indicating fully insulating behavior. The loss of metallicity can be quantified through the integrated spectral weight [15]. Let us define $W = \int_{\omega_1}^{\omega_2} \sigma_1(\omega) d\omega$, where the integral is performed over the frequency range 1400–5200 cm^{-1}, and is shown for all samples in Fig. 3(c). The thickest sample (123 nm) shows a weight of roughly $2 \times 10^6\ \Omega^{-1}\ \text{cm}^{-2}$ only slightly suppressed from bulk, while the weight of the thinnest sample is depressed by an order of magnitude from the bulk value.

The observed changes are apparent in relatively thick (tens of nanometers) samples. Given the incoherent optical response [11] and negligible electronic dispersion [28] along the c axis of BSCCO, we do not expect quantum size effects to be significant. On the other hand, several experiments have demonstrated oxygen depletion from BSCCO surfaces [29,30], and so we attribute the reduced metallic behavior to a more prosaic effect, namely, the escape of oxygen interstitials that causes a region near the surface to become insulating. This suggests that the insulating behavior observed in single unit cell BSCCO [4] is an extrinsic effect. BSCCO is also known to be sensitive to water and so moisture in the air may also play a role in degrading the surface of the two-dimensional atomic crystal samples [31].

IV. EFFECTIVE MEDIUM APPROXIMATION

The scenario of an insulating surface in our exfoliated films points to the interpretation of the optical data through an effective medium approximation (EMA) in which the measured response is a volume average of two different media (in this case an insulating surface and a relatively unperturbed core) [32,33]. For light with frequency $\omega = 2000\ \text{cm}^{-1}$ and vacuum wavelength $\lambda_{\text{vac}} = 5\ \mu\text{m}$, the optical constants of bulk BSCCO yield a refractive index $n \approx 5.8$, meaning the optical wavelength at this frequency is roughly $\lambda = \lambda_{\text{vac}}/n = 855$ nm inside the BSCCO. Since this is an order of magnitude larger than the samples considered here, we can naively consider the samples as consisting of two conductors in parallel. Furthermore, the long wavelength of our probe photons means our measurements are also insensitive to short length-scale variations of the oxygen content, such as at the interface between conducting and insulating regions. The effective complex optical conductivity is then given by $\hat{\sigma}_{\text{EMA}} = f_b\hat{\sigma}_{\text{int}} + (1 - f_b)\hat{\sigma}_{\text{surf}}$. Here $\hat{\sigma}_{\text{int}}$ and $\hat{\sigma}_{\text{surf}}$ are the conductivities of metallic BSCCO and the insulating layer, respectively; f_b is the metallic volume fraction and is equal to $(t - d)/t$, where t is the sample thickness as measured by AFM and d is the thickness of the insulating layer.

To evaluate the validity of this approximation, we return to the spectral weight shown in Fig. 3(c). Taking the real part of σ_{EMA} and integrating yields $W_{\text{EMA}} = f_b W_{\text{bulk}} + (1 - f_b)W_{\text{surf}}$, where W_{bulk} and W_{surf} are the interior and surface spectral weights, respectively. The change of the spectral weight with thickness shown in Fig. 3(c) is well described by this expression (plotted in solid red) assuming physically reasonable values for the insulating layer thickness (d), the insulating layer (W_{surf}), and bulk (W_{bulk}) spectral weights. Fitting these quantities to the data yields values $d = 14.6$ nm, $W_{\text{surf}} = 2 \times 10^5\ \Omega^{-1}\ \text{cm}^{-2}$, and $W_{\text{bulk}} = 2.4 \times 10^6\ \Omega^{-1}\ \text{cm}^{-2}$. The fitted parameters are in agreement with the measured bulk spectral weight, the measured insulating crystal spectral weight, and with the observed onset of insulating behavior in the thinnest (less than 16 nm) samples. This agreement provides strong support for the presence of an insulating surface and for the applicability of the EMA. Indeed, this result also explains the insulating behavior observed in DC transport [4], as the insulating region would be expected to extend throughout the single unit cell thick samples used in that study.

V. CONCLUSIONS

In summary, we have studied the optical properties of exfoliated BSCCO two-dimensional atomic crystals using infrared spectromicroscopy. We observe a progressive suppression of $\sigma_1(\omega)$ in the two-dimensional atomic crystals of BSCCO, with the thinnest specimens showing insulating behavior. The trend in spectral weight indicates that the region extending roughly 15 nm from the surface of the exfoliated BSCCO has a tendency to become insulating. This suggests that the insulating behavior previously observed in 2D atomic crystals of BSCCO is an extrinsic effect [4].

Our results suggest that any devices based on exfoliated BSCCO would likely require steps to prevent or compensate for surface degradation. In particular, the insulating surface layer would be expected to lead to high contact resistance. Possibilities include oxygen annealing or employing a gold capping layer, or else performing the sample preparation and measurement in an inert atmosphere. It would also be helpful to identify the precise cause of the surface degradation. The application of surface analysis techniques, such as x-ray photoelectron spectroscopy or secondary ion mass spectroscopy, is desirable in this regard.

ACKNOWLEDGMENTS

The authors would like to acknowledge the input of Young-June Kim, Andreea Lupascu, and Zhiqiang Li, and thank M. C. Goh for use of her AFM. Research described in this work was performed at the Mid-IR beamline of the Canadian Light Source, which is supported by the Natural Sciences

and Engineering Research Council of Canada, the National Research Council Canada, the Canadian Institutes of Health Research, the Province of Saskatchewan, Western Economic Diversification Canada, and the University of Saskatchewan. Work at Brookhaven is supported by the US DOE under Contract No. DE-AC02-98CH10886.

[1] K. S. Novoselov, A. K. Geim, S. V. Morozov, D. Jiang, Y. Zhang, S. V. Dubonos, I. V. Grigorieva, and A. A. Firsov, Science **306**, 666 (2004).
[2] A. Splendiani, L. Sun, Y. Zhang, T. Li, J. Kim, C.-Y. Chim, G. Galli, and F. Wang, Nano Lett. **10**, 1271 (2010).
[3] J. T. Ye, Y. J. Zhang, R. Akashi, M. S. Bahramy, R. Arita, and Y. Iwasa, Science **338**, 1193 (2012).
[4] K. S. Novoselov, D. Jiang, F. Schedin, T. J. Booth, V. V. Khotkevich, S. V. Morozov, and A. K. Geim, Proc. Natl. Acad. Sci. USA **102**, 10451 (2005).
[5] J. Wei and D. Natelson, Nanoscale **3**, 3509 (2011).
[6] D. Kim, S. Cho, N. P. Butch, P. Syers, K. Kirshenbaum, S. Adam, J. Paglione, and M. S. Fuhrer, Nat. Phys. **8**, 459 (2012).
[7] K. F. Mak, M. Y. Sfeir, J. A. Misewich, and T. F. Heinz, Proc. Natl. Acad. Sci. USA **107**, 14999 (2010).
[8] K. F. Mak, C. Lee, J. Hone, J. Shan, and T. F. Heinz, Phys. Rev. Lett. **105**, 136805 (2010).
[9] A. T. Bollinger, G. Dubuis, J. Yoon, D. Pavuna, J. Misewich, and I. Bozovic, Nature (London) **472**, 458 (2011).
[10] G. Logvenov, A. Gozar, and I. Bozovic, Science **326**, 699 (2009).
[11] D. N. Basov and T. Timusk, Rev. Mod. Phys. **77**, 721 (2005).
[12] D. v. d. Marel, H. J. A. Molegraaf, J. Zaanen, Z. Nussinov, F. Carbone, A. Damascelli, H. Eisaki, M. Greven, P. H. Kes, and M. Li, Nature (London) **425**, 271 (2003).
[13] M. A. Quijada, D. B. Tanner, R. J. Kelley, M. Onellion, H. Berger, and G. Margaritondo, Phys. Rev. B **60**, 14917 (1999).
[14] Z. Q. Li, E. A. Henriksen, Z. Jiang, Z. Hao, M. C. Martin, P. Kim, H. L. Stormer, and D. N. Basov, Nat. Phys. **4**, 532 (2008).
[15] D. N. Basov, R. D. Averitt, D. van der Marel, M. Dressel, and K. Haule, Rev. Mod. Phys. **83**, 471 (2011).
[16] L. J. Sandilands, J. X. Shen, G. M. Chugunov, S. Y. F. Zhao, S. Ono, Y. Ando, and K. S. Burch, Phys. Rev. B **82**, 064503 (2010).
[17] S. Y. F. Zhao, C. Beekman, L. J. Sandilands, J. E. J. Bashucky, D. Kwok, N. Lee, A. D. LaForge, S. W. Cheong, and K. S. Burch, Appl. Phys. Lett. **98**, 141911 (2011).
[18] J. S. Wen, Z. J. Xu, G. Y. Xu, M. Hücker, J. M. Tranquada, and G. D. Gu, J. Cryst. Growth **310**, 1401 (2008).
[19] X. Wang, L. X. You, X. M. Xie, C. T. Lin, and M. H. Jiang, J. Raman Spectrosc. **43**, 949 (2012).
[20] A. Lupascu, R. Feng, L. J. Sandilands, Z. Nie, V. Baydina, G. Gu, S. Ono, Y. Ando, D. C. Kwok, N. Lee, S.-W. Cheong, K. S. Burch, and Y.-J. Kim, Appl. Phys. Lett. **101**, 223106 (2012).
[21] A. A. Reijnders, Y. Tian, L. J. Sandilands, G. Pohl, I. D. Kivlichan, S. Y. Frank Zhao, S. Jia, M. E. Charles, R. J. Cava, N. Alidoust, S. Xu, M. Neupane, M. Z. Hasan, X. Wang, S. W. Cheong, and K. S. Burch, Phys. Rev. B **89**, 075138 (2014).
[22] C. C. Homes, M. Reedyk, D. A. Cradles, and T. Timusk, Appl. Opt. **32**, 2976 (1993).
[23] J. Hwang, T. Timusk, and G. D. Gu, J. Phys.: Condens. Matter **19**, 125208 (2007).
[24] *Handbook of Optical Constants*, edited by E. Palik (Academic, New York, 1998), Vol. 1, pp. 547–569 and 749–763.
[25] A. Kuzmenko, REFFIT: Software to fit optical spectra, http://optics.unige.ch/alexey/reffit.html.
[26] A. B. Kuzmenko, Rev. Sci. Instrum. **76**, 083108 (2005).
[27] M. Dressel and G. Grüner, *Electrodynamics of Solids: Optical Properties of Electrons in Matter* (Cambridge University Press, Cambridge, UK, 2002).
[28] T. Takeuchi, T. Kondo, T. Kitao, H. Kaga, H. Yang, H. Ding, A. Kaminski, and J. C. Campuzano, Phys. Rev. Lett. **95**, 227004 (2005).
[29] M. Truccato, C. Lamberti, C. Prestipino, and A. Agostino, Appl. Phys. Lett. **86**, 213116 (2005).
[30] S. Saito, Y. Uhara, Y. Kogushi, H. Yoshida, S. Isono, H. Yamasaki, H. Murakami, T. Sutou, T. Soumura, and T. Kioka, Phys. Status Solidi A **202**, R129 (2005).
[31] K. Yoshikawa, M. Yoshida, and M. Nakano, Jpn. J. Appl. Phys. **27**, L2324 (1988).
[32] K. S. Burch, E. J. Singley, J. Stephens, R. K. Kawakami, D. D. Awschalom, and D. N. Basov, Phys. Rev. B **71**, 125340 (2005).
[33] D. Aspnes, Thin Solid Films **89**, 249 (1982).